УДК 691.714, 539.26
P.A.C.S. 61.72.Mm, 61.05.C−

DOI 10.54708/26587572_2025_732287

MICROSTRUCTURE AND PROPERTIES OF 09G2S STEEL PROCESSED BY EQUAL-CHANNEL ANGULAR PRESSING

Andrey Vladimirovich Malinin [1], Artem Anatolievich Nikolaev [1], Vil Dayanovich Sitdikov [1, 2]

[1] LLC RN – BashNIPIneft (subsidiary of PJSC Rosneft), 86/1 Lenin st., 450076 Ufa, Russia
[2] Institute for Metals Superplasticity Problems of the Russian Academy of Sciences, 39 Stepana Khalturina st., 450001 Ufa, Russia
[a] SitdikovVD@bnipi.rosneft.ru

ABSTRACT

The effect of equal-channel angular pressing (ECAP) on the microstructure, mechanical, and corrosion properties of low-carbon 09G2S steel was investigated. It was established that ECAP processing leads to the formation of an ultrafine-grained (UFG) state, accompanied by ferrite grain refinement, an increase in dislocation density, fragmentation, and partial dissolution of cementite, as well as an increase in the fraction of globular carbide phases. These changes were analyzed in detail using electron microscopy and X-ray diffraction techniques. After four ECAP passes, the average ferrite grain size decreased from 11 μm to ~560 nm. Phase analysis revealed a redistribution of carbide precipitates: the mass fraction of lamellar cementite (Fe_3C) decreased, while the content of globular particles $Mn_{23}C_6$, Mn_7C_3, and Cr_3C_2 increased. X-ray line profile analysis performed by the modified Williamson-Hall and Warren-Averbach methods demonstrated grain refinement and increased dislocation density. According to the modified Williamson-Hall approach, the dislocation density increased from 1×10^{13} m^{-2} in the initial state to 1.5×10^{13} m^{-2} after four ECAP passes, while the size of coherent scattering domains decreased more than fourfold. The modified Warren-Averbach method showed comparable trends. Corrosion tests indicated that the formation of the UFG structure was accompanied by an approximately 1.3 fold increase in corrosion rate. It is concluded that the improvement in strength and the reduction in corrosion resistance of 09G2S steel are associated with grain refinement, an increase in grain boundary area, high defect density, and the redistribution of carbide phases.

KEYWORDS

Low-carbon steel; ferrite; equal channel angular pressing; ultrafine grain structure; microstructure; strengthening mechanisms; X-ray diffraction analysis.

МИКРОСТРУКТУРА И СВОЙСТВА СТАЛИ 09Г2С, ОБРАБОТАННОЙ МЕТОДОМ РАВНОКАНАЛЬНОГО УГЛОВОГО ПРЕССОВАНИЯ

Андрей Владимирович Малинин [1], Артем Анатольевич Николаев [1], Виль Даянович Ситдиков [1, 2]

[1] ООО «РН-БашНИПИнефть» (дочернее общество ПАО «Роснефть»), Россия, 450076 г. Уфа, ул. Ленина, 86/1
[2] Институт проблем сверхпластичности металлов Российской академии наук, Россия, 450001 г. Уфа, ул. Степана Халтурина, 39
[a] SitdikovVD@bnipi.rosneft.ru

АННОТАЦИЯ

В работе исследовано влияние равноканального углового прессования (РКУП) на структуру, прочностные и коррозионные свойства низкоуглеродистой стали 09Г2С. Установлено, что в процессе РКУП обработки формируется ультрамелкозернистое (УМЗ) состояние, сопровождающееся измельчением ферритных зерен, повышением плотности внесенных дислокаций, фрагментацией и частичным растворением цементита, а также увеличением содержания карбидных фаз глобулярной формы. Эти изменения детально проанализированы как методом электронной микроскопии, так и методами рентгеновской дифрактометрии. Показано, что в результате четырех проходов РКУП обработки стали средний размер ферритных зерен уменьшается с 11 мкм до ~560 нм. Фазовый анализ выявил перераспределение карбидных выделений, при котором массовая доля пластинчатого цементита (Fe_3C) уменьшается, а содержание глобулярных частиц $Mn_{23}C_6$, Mn_7C_3 и Cr_3C_2 увеличивается. Данные рентгеноструктурного анализа, полученные модифицированными методами Вильямсона-Холла и Уоррена-Авербаха показали измельчение зеренной структуры и повышение плотности дислокаций. По модифицированному методу Вильямсона-Холла плотность дислокаций возрастает с 1×10^{13} м$^{-2}$ в исходном состоянии до $1{,}5\times10^{15}$ м$^{-2}$, а размер областей когерентного рассеяния уменьшается более чем в шесть раз после четырех проходов РКУП. Модифицированный метод Уоррена-Авербаха показал сопоставимые тенденции. Коррозионные испытания показали, что формирование УМЗ структуры сопровождается увеличением скорости коррозии примерно в 1,3 раза. Сделан вывод о том, что повышение прочностных свойств и понижение коррозионной стойкости стали 09Г2С связано с измельчением зеренной структуры, ростом доли границ зерен, высокой плотностью дефектов и перераспределением карбидных фаз.

КЛЮЧЕВЫЕ СЛОВА

Низкоуглеродистая сталь; феррит; равноканально-угловое прессование; ультрамелкозернистая структура; микроструктура; механизмы упрочнения; рентгеноструктурный анализ.

Introduction

In modern materials science, considerable attention is devoted to the development of methods for controlling the microstructure and optimizing the physical and mechanical properties of low-alloy structural steels. Among various thermomechanical treatment techniques, one of the most effective approaches for improving the performance of steels is the formation of ultrafine-grained (UFG) structures, which provide a combination of high strength, good ductility, and wear resistance [1–3]. Over the past decades, severe plastic deformation (SPD) has established itself as a versatile tool for producing UFG states in metals and alloys [4–6]. Among the different SPD techniques, equal-channel angular pressing (ECAP) occupies a special place, as it enables the introduction of large plastic strains into samples without altering their geometric dimensions [1–6].

Earlier studies have shown that ECAP processing effectively refines the grain structure, leading to a significant increase in strength in aluminum, titanium, and magnesium alloys [7–9], as well as in several structural steels [10, 11]. However, in low-alloy steels widely used in the oil industry, detailed X-ray investigations of the microstructural and phase evolution under ECAP remain limited. Of particular interest are the processes of cementite fragmentation and dissolution, the degree of grain refinement and defect accumulation, as well as the precipitation and further evolution of carbide phases ($Me_{23}C_6$, Me_7C_3, Me_3C_2, etc.), which can significantly affect both the mechanical properties and corrosion resistance of the material [12–14].

Table 1. Chemical composition of 09G2S steel (wt.%)

Таблица 1. Химический состав стали 09Г2С (мас.%)

C	Mn	Si	Cr	Ni	Cu	Mo	S	P	Fe
0.09	1.63	0.77	0.27	0.22	0.18	0.05%	0.02	0.01	bal.

Alongside strength properties, the corrosion resistance of steels under downhole service conditions is of practical importance. According to previous studies [15–17], the formation of UFG structures may either enhance or deteriorate corrosion behavior depending on the alloy, the environment, and the nature of secondary phases. For 09G2S steel, which is widely used in the oil industry for tubing applications in downhole environments, data on the influence of ECAP on its corrosion performance are virtually absent. Therefore, a comprehensive investigation of the effect of ECAP on the microstructure, phase composition, mechanical properties, and corrosion resistance of low-alloy 09G2S steel is of particular relevance.

The aim of this work is to study the evolution of the microstructure and phase composition of 09G2S steel during ECAP processing using electron microscopy and X-ray diffraction analysis, and to establish the relationship between structural changes, mechanical properties, and corrosion resistance.

1. Materials and methods

The material selected for this study was 09G2S steel, with its chemical composition presented in Table 1. To obtain an UFG structure, cylindrical billets (9 mm in diameter and 30 mm in length) were prepared. Prior to ECAP processing, the samples were normalized at 950 °C for 0.5 h. ECAP with an intersection angle of 120° was performed at 200 °C for up to four passes, corresponding to an equivalent strain of ~2.67.

Mechanical properties (yield strength σ_{YS}, ultimate tensile strength σ_{UTS}, and elongation δ) of both coarse-grained CG and UFG steels were determined by tensile testing using a universal testing machine (Instron 8801). The tests were carried out on miniature flat specimens with a thickness of 1 mm, a gauge length of 4 mm, and cross-sectional dimensions of 1×1 mm^2. The strain rate during testing was 1×10^{-3} s^{-1}. The corrosion rate of the steel was measured by the weight loss method after exposing disk-shaped samples (9 mm in diameter, 2 mm in thickness) in a corrosive medium (5.0 wt.% NaCl, 0.5 wt.% acetic acid, distilled water) for 100 days. The microstructure of the as-received and ECAP-processed specimens (after 2 and 4 passes) was examined using a scanning electron microscope (SEM), (Thermo Scientific Q250) and an X-ray diffractometer (Tongda TD-3000). X-ray diffraction (XRD) patterns were recorded over a 2θ range of 20–145° at a scanning rate of 0.5°/min, using Cu Kα radiation generated at 40 kV and 35 mA.

The fine structural parameters including the average size D of coherent scattering domains (CSD), dislocation density ρ, effective outer cut-off radius R_e, and the fraction of screw dislocations f_s were calculated using modified Williamson-Hall (mW-H) and Warren-Averbach (mW-A) methods [18]. In the mW-H approach, the CSD size D_{WH}, dislocation density ρ_{WH}, and the fraction of screw dislocations were determined from the full width at half maximum (FWHM) broadening of diffraction peaks according to the relation: $\Delta K = \mathrm{FWHM}\cdot\cos\theta/\lambda$ vs. $K = 2\sin\theta/\lambda$:

$$\frac{\Delta K^2 - \alpha^2}{K^2} = \frac{\pi M^2 b^2}{2}\rho_{WH}\overline{C}_{hoo}\left(1 - qH^2\right). \quad (1)$$

Here, K is the scattering vector, $\alpha = \frac{0.9}{D_{WH}}$, M is the Wilkens parameter, which depends on the effective outer cut-off radius R_e of dislocations, b is the Burgers vector, λ is the X-ray

wavelength, and $\overline{C}_{hoo}$ is the average dislocation contrast factor for the (h00) reflection. The expression $\overline{C}_{hoo}(1-qH^2)=\overline{C}_{hkl}$ represents the averaged dislocation contrast factor, where q defines the dislocation character, and $H^2=(h^2k^2+h^2l^2+l^2k^2)/(h^2+k^2+l^2)$. In the mW-A method, the dislocation density ρ_{WA}, effective outer cut-off radius R_e, and Wilkens parameter M were also determined from the real A(L) and size-dependent $A^s(L)$ Fourier coefficients (where L is the Fourier length) obtained from the decomposition of the diffraction line profile:

$$\ln A(L) = \ln A^s(L) - \frac{\pi b^2 \rho_{W-A}^{1/2}}{2} L^2 \ln\left(\frac{R_e}{L}\right)\left(K^2\overline{C}\right) = \ln A^S(L) - YK^2\overline{C}. \quad (2)$$

After transforming the variable y, the following relation was obtained for determining ρ_{WA} и R_e:

$$\frac{Y}{L^2} = \rho_{WA}^{1/2}\frac{\pi b^2}{2}\ln(R_e) - \rho_{WA}^{1/2}\frac{\pi b^2}{2}\ln(L). \quad (3)$$

The contribution of instrumental broadening to the diffraction line profiles in the above methods was taken into account by recording and analyzing the diffraction pattern of LaB_6 powder.

2. Results

The results of tensile tests and corrosion rate measurements for the as-received and ECAP processed steel are presented in Table 2. The analysis shows that an increase in the number of ECAP passes significantly enhances the strength characteristics of the material. After two passes, both yield strength and ultimate tensile strength increased by approximately 1.7 times compared to the initial state, and after four passes they more than doubled. At the same time, the ductility of the steel decreased noticeably. The tests also revealed an increase in corrosion rate: in the UFG state (after four passes), it rose by about 1.3 times (Table 2).

Fig. 1 shows SEM images of the steel microstructure in the as-received state and after ECAP processing. In the initial condition, ferrite-pearlite grains are observed (Fig. 1, *a*). The average ferrite grain size is 11 μm, while the pearlite colonies have an average size of 8 μm. The mean spacing between lamellar cementite (Fe_3C) particles is 0.6 μm, with an average thickness of ~95 nm. In addition to lamellar cementite, globular particles identified by phase analysis (see below) as $Me_{23}C_6$, Me_7C_3 and Me_3C_2 are also present, occurring both in ferrite and pearlite grains.

Table 2. Mechanical properties and corrosion rate of the as-received and ECAP processed steel

Таблица 2. Механические свойства и скорость коррозии стали в состоянии поставки и после равноканального углового прессования

State / Состояние	Yield strength, MPa / Предел текучести, МПа	Ultimate tensile strength, MPa / Предел прочности при растяжении, МПа	Elongation, % / Удлинение, %	Corrosion rate, mm/year / Скорость коррозии, мм/год
As-received / Поставки	473±12	581±9	16±1	0.208±0.04
ECAP, 2 passes / РКУП, 2 прохода	867±9	976±10	9±1	0.236±0.04
ECAP, 4 passes / РКУП, 4 прохода	979±10	1192±11	7±1	0.269±0.04

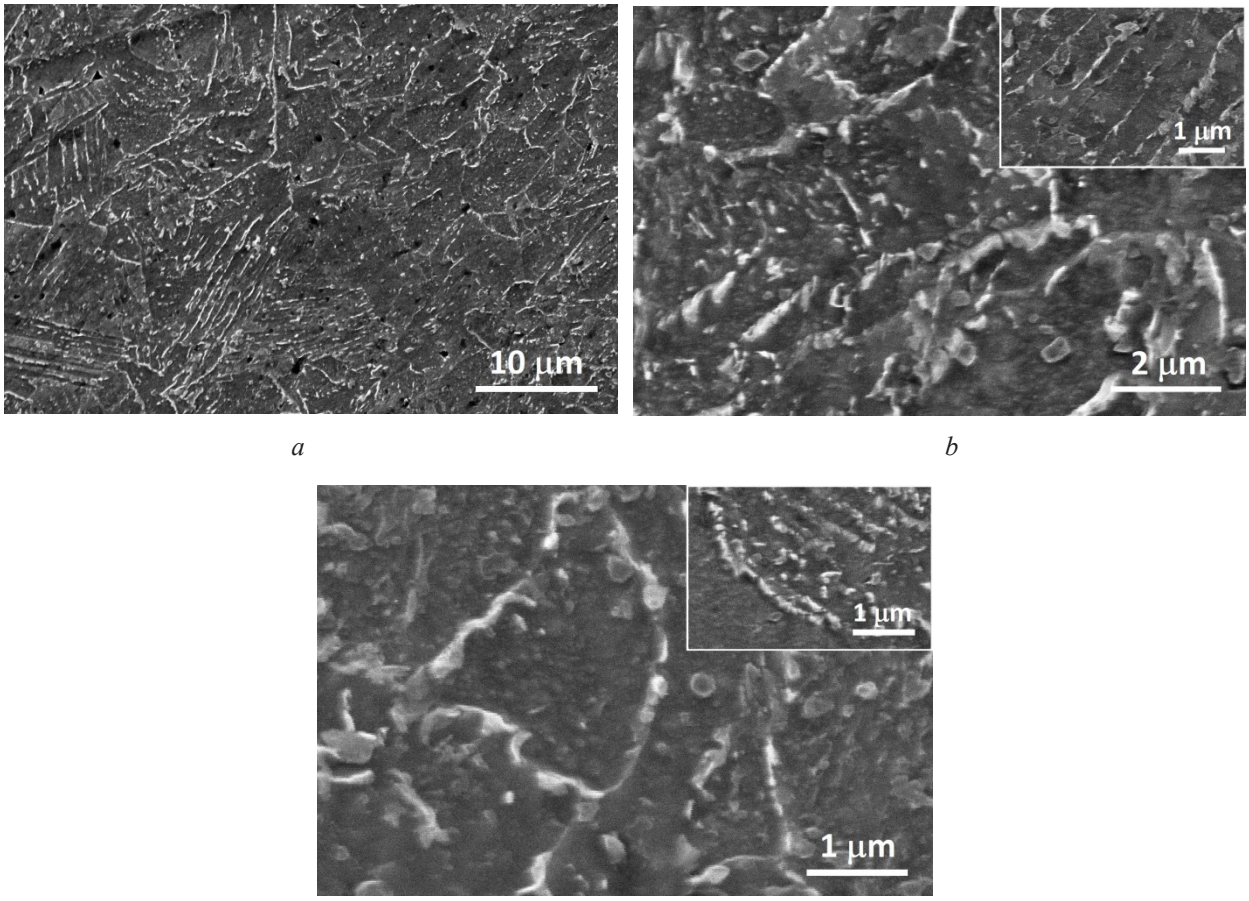

a *b* *c*

Fig. 1. SEM images of the microstructure of 09G2S steel in the as-received state (*a*), after 2 ECAP passes (*b*), and after 4 ECAP passes (*c*). Insets show pearlite regions

Рис. 1. СЭМ-изображения микроструктуры стали 09Г2С в состоянии поставки (*a*), после 2 проходов РКУП (*b*) и после 4 проходов РКУП (*c*). На вставках показаны области перлита

After two ECAP passes, a noticeable refinement of the structure takes place (Fig. 1, *b*): the average ferrite grain size decreases to 770 nm, cementite lamellae within pearlite colonies become fragmented and thickened, and partial dissolution of cementite is observed in some regions. After four passes, the refinement continues (Fig. 1, *c*), with the average ferrite grain size reduced to 560 nm. At the same time, globular carbides such as $Me_{23}C_6$, Me_7C_3 and Me_3C_2 grow in size, while lamellar cementite undergoes further fragmentation and dissolution (Fig. 1, *c*, inset).

Fig. 2 presents the XRD patterns of the steel in different structural states, along with an example of diffraction spectrum analysis after four ECAP passes. In the initial state, the diffraction pattern is characterized by a set of intense α-Fe (ferrite) reflections and weak peaks corresponding to Fe_3C, $Mn_{23}C_6$, and Mn_7C_3 phases. After two ECAP passes, in addition to these phases, reflections of Cr_3C_2 are also observed. With increasing number of passes up to four, the intensity of peaks from secondary phases increases. According to electron microscopy data (Fig. 1), these precipitates correspond to lamellar cementite (Fe_3C) as well as globular carbides $Mn_{23}C_6$, Mn_7C_3, and Cr_3C_2. Quantitative analysis of their content was carried out using the Rietveld method. An example of diffraction pattern refinement after four ECAP passes is shown in Fig. 2, *b*, and the calculated phase fractions are summarized in Table 3. During the Rietveld analysis, the lattice parameter was also determined.

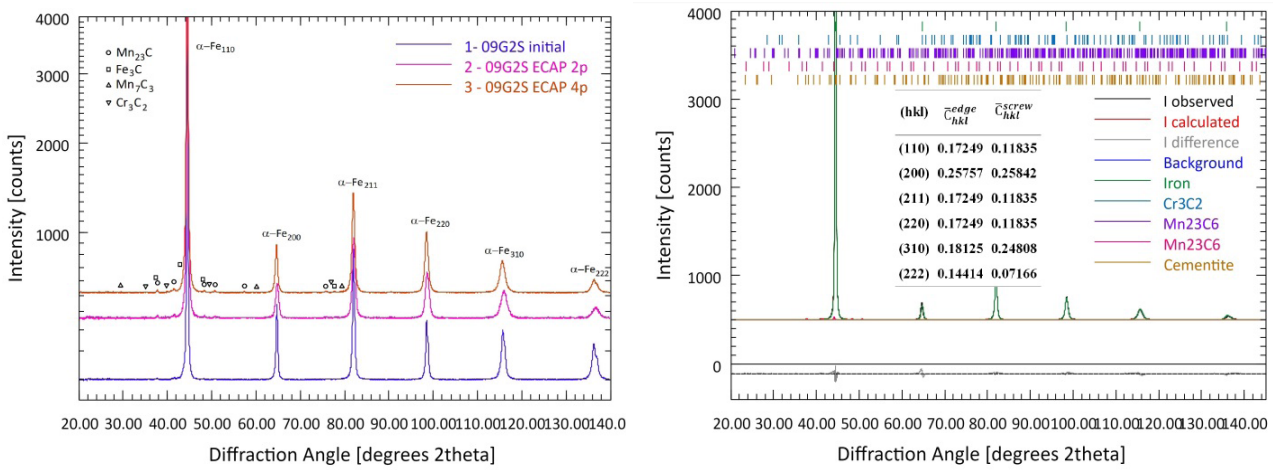

a *b*

Fig. 2. XRD patterns of 09G2S steel in different structural states (*a*) and refined diffraction pattern of the steel after 4 ECAP passes (*b*)

Рис. 2. Рентгеновские дифрактограммы стали 09Г2С в различных структурных состояниях (*a*) и уточненная дифрактограмма стали после 4 проходов РКУП (*b*)

Analysis of the data in Table 3 shows that in the as-received steel, lamellar cementite particles predominate. After two ECAP passes, their mass fraction decreases, while the content of $Mn_{23}C_6$ and Mn_7C_3 carbides increases, and the appearance of the Cr_3C_2 phase is detected. After four passes, a further reduction in the Fe_3C fraction and an increase in the amount of globular carbides were observed. The processes of lamellar cementite dissolution (i.e., the reduction in Fe_3C content) were also confirmed by the SEM images (Fig. 1, *b, c*). By analyzing the broadening of diffraction lines and using equations (1)–(3), the X-ray line profile analysis (XLPA) parameters of the fine structure of the steel were determined. The analysis was performed for the ferrite (α-Fe) phase, assuming the presence of a small amount of alloying elements in this phase. First, following the methodology in [19], the contrast factors $\overline{C}_{hkl}^{edge}$ for edge dislocations and $\overline{C}_{hkl}^{screw}$ for screw dislocations were calculated (Fig. 2, *b*). Based on these data, the values $q^s = 2.46$ and $q^e = 1.33$ were obtained. The elastic constants C_{11}, C_{12}, and C_{44} used in the calculations were taken from [20] for α-Fe.

To determine the parameter q, the coefficient α in equation (1) was varied until a linear dependence was obtained (Fig. 3, *a*). Then, using the mW-H method, the intercept of the curve with the OX axis was found, and q was calculated according to the formula $q = 1/H^2$. The obtained values were 1.82 for the as-received state, 1.72 after two ECAP passes, and 1.66 after four passes. According to the relation $q = (1 - f_s)q^e + f_s q^s$, the fraction of screw dislocations f_s was calculated (Table 4).

Table 3. Identified phases and their content in the as-received and ECAP processed steel

Таблица 3. Выявленные фазы и их содержание в стали в состоянии поставки и после РКУП

State	Mass fraction of precipitates, %			
	Fe_3C	$Mn_{23}C_6$	Mn_7C_3	Cr_3C_2
As-received	1.05	0.21	0.10	0.00
ECAP, 2 passes	0.45	0.47	0.18	0.11
ECAP, 4 passes	0.17	0.68	0.24	0.19

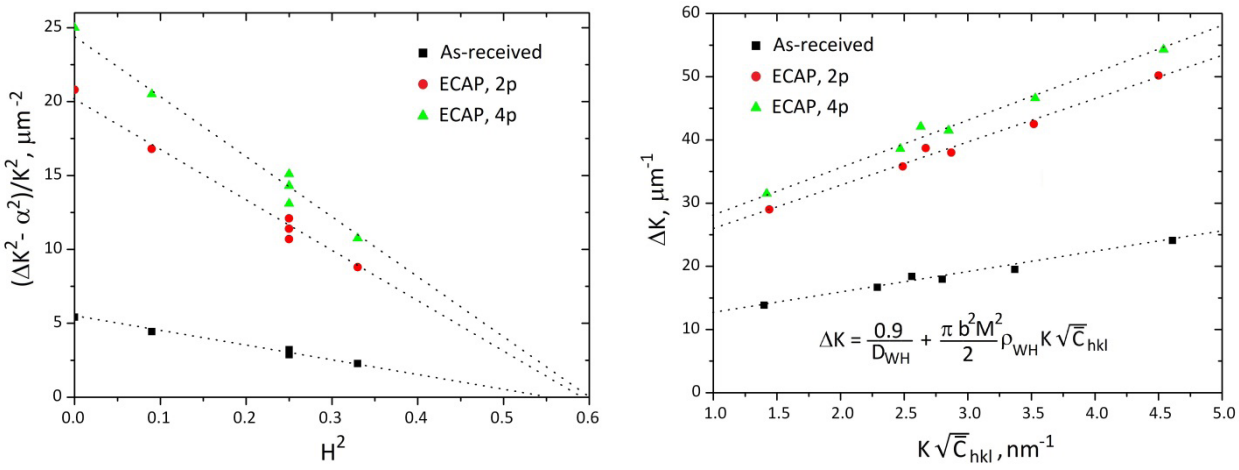

a *b*

Fig. 3. Experimental dependences for different structural states of 09G2S steel obtained by the modified Williamson-Hall method:

a – $(\Delta K^2 - \alpha^2)/K^2$ versus H^2; b – ΔK versus $K\sqrt{\bar{C}_{hkl}}$

Рис. 3. Экспериментальные зависимости для различных структ. состояний стали 09Г2С, полученные модифицированным методом Вильямсона-Холла:

a – $(\Delta K^2 - \alpha^2)/K^2$ от H^2; b – ΔK от $K\sqrt{\bar{C}_{hkl}}$

The coherent scattering domain size D_{WH} of the steel in different structural states was determined from the dependence of ΔK on $K\sqrt{\bar{C}_{hkl}}$. By extrapolating these dependences to $K\sqrt{\bar{C}_{hkl}} = 0$, the values of ΔK_i were obtained, after which the CSD size was calculated using $D_{WH} = 1/\Delta K_i$ (Table 4). The dislocation density ρ_{WA} was determined from the slope of the ΔK versus $K\sqrt{\bar{C}_{hkl}}$ plot (Fig. 3, *b*).

To determine the remaining fine-structural parameters of the as-received and ECAP-processed steel, Fourier analysis of all diffraction peaks was performed. The obtained Fourier coefficients were used in the mW-A method. Some of the dependences calculated by this method are presented in Fig. 4. The dependences of lnA(L) on $K^2\bar{C}$ (Fig. 4, *a, b*) were extrapolated to the OY axis intercept, from which the size coefficients $A^s(L)$ were determined for the studied states of steel (Fig. 4, *c*).

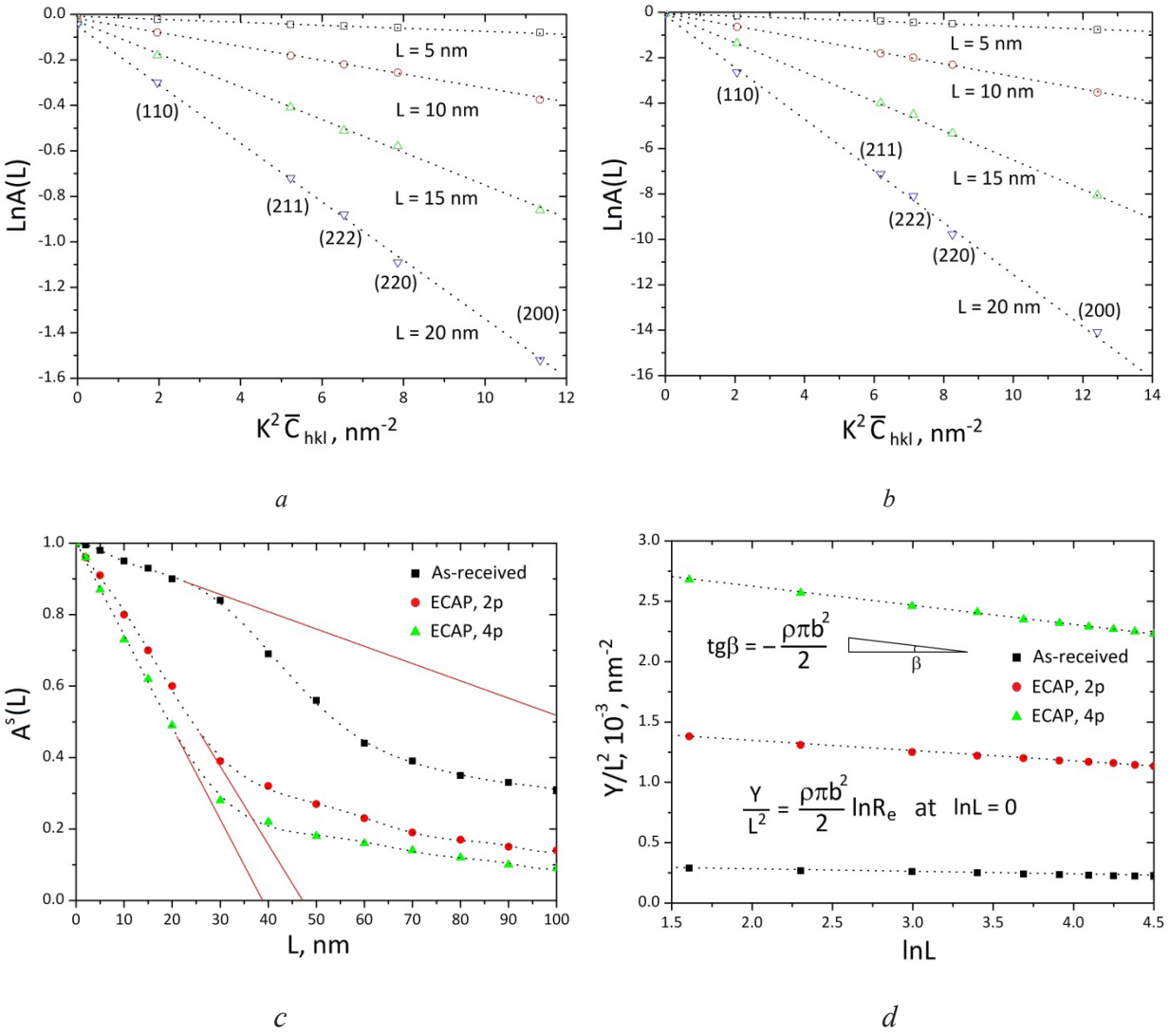

Fig. 4. Experimental dependences for different structural states of 09G2S steel obtained by the modified Warren-Averbach method:
a, b – lnA(L) versus $K^2\overline{C}$ for the as-received and ECAPed steel (4 passes); c – $A^s(L)$ versus L; d – Y/L^2 versus lnL

Рис. 4. Экспериментальные зависимости для различных структурных состояний стали 09Г2С, полученные модифицированным методом Уоррена-Авербаха:
a, b – lnA(L) от $K^2\overline{C}$ для стали в состоянии поставки и после РКУП (4 прохода); c – $A^s(L)$ от L; d – Y/L^2 от lnL

In all graphs, the dependence of $A^s(L)$ on L in the region of L below ~30 nm exhibited a linear behavior. Further extrapolation to the point where $A^s(L) = 0$ made it possible to determine the coherent scattering domain size D_{WA} (Table 4). The extrapolation lines in Fig. 4, *c* are shown in red. From the dependences of lnA(L) on $K^2\overline{C}$, the values of Y for different steel states were additionally determined. These data were substituted into equation (3) to construct the dependence of Y/L^2 on lnL (Fig. 4, *d*). Based on the obtained plots, the dislocation density ρ_{WA} and the effective outer cut-off radius of dislocations R_e were calculated (Table 4). All XLPA parameters of the steel microstructure in different structural states are summarized in Table 4.

Table 4. XLPA parameters* of the steel microstructure in the as-received and ECAP processed states

Таблица 4. Параметры* АПРЛ микроструктуры стали в состоянии поставки и после РКУП

State	a, nm	D_{WH}, nm	D_{WA}, nm	f_s, %	ρ_{WH}, 10^{14} m^{-2}	ρ_{WA}, 10^{14} m^{-2}	R_e, nm	M
As-received	2.876016(2)	244	191	43%	0.1	3.5	225	4.2
ECAP, 2 passes	2.875877(2)	58	38	34%	11.5	13.0	20	0.74
ECAP, 4 passes	2.875793(1)	51	47	29%	15.0	24.3	9	0.45

**a – lattice parameter; D_{WH} – CSD size from mW-H method; D_{WA} – CSD size from mW-A method; ρ_{WH} – dislocation density from mW-H method; ρ_{WA} – dislocation density from mW-A method; f_s – fraction of screw dislocations; R_e – effective outer cut-off radius of dislocations; M – Wilkens parameter*

**a – параметр решетки; D_{WH} – размер области когерентного рассеяния согласно модиф. методу Вильямсона-Холла; D_{WA} – размер ОКР согласно модиф. методу Уоррена-Авербаха; ρ_{WH} – плотность дислокаций согласно модиф. методу Вильямсона-Холла; ρ_{WA} – плотность дислокаций согласно модиф. методу Уоррена-Авербаха; f_s – доля винтовых дислокаций; R_e – эффективный внешний радиус обрезания дислокаций; M – параметр Вилкенса*

Analysis of Table 4 shows that ECAP processing leads to a decrease in the lattice parameter, a reduction in the size of coherent scattering domains, an increase in dislocation density, and a reduction in the fraction of screw dislocations. At the same time, the decrease in R_e and M values indicates the development of dislocation dipole fields and a transition toward a more ordered arrangement of dislocations.

3. Discussion

The conducted studies have shown that ECAP processing significantly modifies the microstructure and properties of low-alloy 09G2S steel. The formation of an UFG state is accompanied by a complex set of interrelated processes, namely, the refinement of ferrite and pearlite grains, fragmentation and partial dissolution of cementite, as well as the redistribution of carbide phases $Mn_{23}C_6$, Mn_7C_3, and Cr_3C_2. These processes result in a substantial increase in strength characteristics (Table 2). In particular, yield strength and ultimate tensile strength more than doubled after four ECAP passes. At the same time, ductility decreased, which is typical of UFG materials where a significant portion of deformation is localized at grain boundaries.

The main strengthening mechanisms in UFG steel are grain boundary strengthening (Hall-Petch effect), strengthening due to increased dislocation density, and precipitation hardening by carbide particles. The XLPA results (Table 4) confirm the sharp increase in dislocation density, reduction in coherent scattering domain size (proportional to grain size), and carbide precipitation (Table 3) during ECAP. According to the mW-A method, the dislocation density increased from 3.5×10^{14} m^{-2} in the initial state to 24.3×10^{14} m^{-2} after four ECAP passes, while D_{WH} decreased more than fourfold (Table 5). Analysis of the corresponding diffraction patterns by the mW-H method revealed similar trends, though the numerical values were lower, which can be explained by differences in sensitivity and methodology. The mW-H method is based on an averaged approximation of line broadening and is less sensitive to the inhomogeneity of defect distribution within grains, resulting in an overestimation of CSD size and underestimation of dislocation density. In contrast, the mW-A method, which is based on Fourier analysis of diffraction line profiles, accounts for local stress variations and peak asymmetry, thus, providing lower CSD sizes and higher dislocation

densities. The discrepancy between the two methods is consistent with literature data [21, 22] and reflects their different sensitivities to size and strain contributions to line broadening. Using both approaches together provides a more comprehensive description of the fine structure of steel after ECAP, allowing reliable evaluation of both the degree of grain refinement and the defect structure.

The formation of the UFG structure in steel is also accompanied by a decrease in the ferrite lattice parameter (Table 4), which can be attributed to a combination of microstructural changes. Primarily, this is related to the emergence of local compressive stress fields, leading to a reduction in interatomic spacing as a result of increased dislocation density and the formation of long-range internal stresses. Additional contributions come from phase transformations occurring during ECAP. Partial dissolution of lamellar cementite is associated with the redistribution of carbon and alloying elements (Mn, Cr) between the ferrite matrix and carbide precipitates. The formation of nonequilibrium grain boundaries also contributes to lattice "contraction" by increasing the free energy of the system. Similar effects of lattice parameter reduction under severe plastic deformation have been reported in [2, 12, 21], where dislocation accumulation and redistribution of interstitial and substitutional atoms were identified as key factors.

A significant reduction in the Wilkens parameter M ($M << 1$) with increasing ECAP passes was also observed. According to [23–25], this parameter reflects the distribution of defects in the crystal lattice and is related to the ordering of the dislocation structure. Its decrease is explained by the growth of dislocation density, grain refinement, and enhanced fragmentation and dissolution of cementite particles, which promote the formation of ordered dislocation arrangements, such as tangles, walls, and cell structures. Similar trends in M reduction under SPD were reported for aluminum and titanium alloys, where it was associated with the transition to UFG structures and the formation of nonequilibrium grain boundaries [26, 27].

Particular attention should be paid to the corrosion behavior. It was established that the corrosion rate of steel increased by about 1.3 times with the number of ECAP passes. This is most likely due to the increased specific grain boundary area, high defect density, and increased carbide precipitation. According to the literature [2, 28], UFG grain boundaries and high dislocation density act as active sites for the initiation and development of corrosion processes. Thus, although ECAP strengthens 09G2S steel through grain refinement, defect accumulation, and carbide precipitation, these structural changes reduce its corrosion resistance.

Overall, the results demonstrate that ECAP is an effective method for producing UFG structures in low-alloy steels, providing significant strengthening through grain refinement, increased defect density, and carbide precipitation. However, these structural changes are accompanied by reduced ductility and corrosion resistance, which must be taken into account for the practical application of 09G2S steel.

Conclusions

The present study has shown that the application of ECAP to low-alloy 09G2S steel leads to the formation of a UFG structure, an increase in dislocation density, and the precipitation and growth of $Mn_{23}C_6$, Mn_7C_3, and Cr_3C_2 carbides. These changes result in more than a twofold increase in strength characteristics; however, they are accompanied by reduced ductility and increased corrosion rate. The findings highlight the necessity of a comprehensive approach to the practical use of UFG steels. For applications under aggressive conditions (such as downhole environments), ECAP should be complemented by subsequent thermomechanical treatment aimed at improving ductility and corrosion resistance.

Acknowledgments / Благодарности

The authors express their gratitude to Rosneft PJSC and RN-BashNIPIneft LLC for the opportunity to conduct the research. The authors also thank A. I. Voloshin, Yu. B. Lind, and N. R. Yarkeeva (RN-BashNIPIneft) for discussing the results obtained and valuable comments during the preparation of the article.

Авторы выражают благодарность ПАО «НК «Роснефть» и ООО «РН-БашНИПИнефть» за предоставленную возможность проведения исследований. Авторы также благодарят доктора химических наук А.И. Волошина, кандидата физико-математических наук Ю.Б. Линд, кандидата технических наук Н.Р. Яркееву (ООО «РН-БашНИПИнефть») за обсуждение полученных результатов и ценные замечания при подготовке статьи.

REFERENCES

1. Valiev R.Z., Islamgaliev R.K., Alexandrov I.V. Bulk nanostructured materials from severe plastic deformation // Progress in Material Science. 2000. Vol. 45. P. 103–189 DOI: 10.1016/S0079-6425(99)00007-9.

2. Valiev R.Z., Langdon T.G. Principles of equal-channel angular pressing as a processing tool for grain refinement // Progress in Material Science. 2006. Vol. 51. P. 881–981. DOI: 10.1016/j.pmatsci.2006.02.003.

3. Prithivirajan S., Gajanan M. N., Narendranath S., Desai V. Recent progress in equal channel angular pressing of magnesium alloys starting from Segal's idea to advancements till date – A review // International Journal of Lightweight Materials and Manufacture. 2023. Vol. 6. P. 82–107. DOI:10.1016/j.ijlmm.2022.08.001.

4. Segal V.M. Equal channel angular extrusion: from macromechanics to structure formation // Material Science and Engineering: A. 1999. Vol. 271. P. 322–333. DOI: 10.1016/S0921-5093(99)00248-8.

5. Estrin Y., Vinogradov A. Extreme grain refinement by severe plastic deformation: a wealth of challenging science // Acta Materialia. 2013. Vol. 61. P. 782–817. DOI: 10.1016/j.actamat.2012.10.038.

6. Iwahashi Y., Horita Z., Nemoto M., Langdon T.G. The process of grain refinement in equal-channel angular pressing // Acta Materialia. 1998. Vol. 46. P. 3317–3331. DOI: 10.1016/S1359-6454(97)00494-1.

7. Awasthi A., Gupta A., Saxena K., Diwedi R.K. Equal channel angular processing on aluminium and its alloys – A review // Materials Today: Proceedings. 2022. Vol. 56. P. 2388–2391. DOI: 10.1016/j.matpr.2021.12.207.

8. Zhao Y., Guo H., Fu M.W., Ning Y., Yao Z. Fabrication of bulk ultrafine grained titanium alloy via equal channel angular pressing based thermomechanical treatment // Materials & Design. 2013Vol. 46. P. 1980-2015. DOI: 10.1016/j.matdes.2012.11.047.

9. Hashemi M., Alizadeh R., Langdon T.G. Recent advances using equal-channel angular pressing to improve the properties of biodegradable Mg–Zn alloys // Journal of Magnesium and Alloys. 2023. Vol. 11. P. 2260–2284. DOI: 10.1016/j.jma.2023.07.009.

10. Borisova M.Z. Strength increase of a low-carbon steel by equal channel angular pressing // Procedia Structural Integrity. 2020. Vol. 30. P. 17–22. DOI: 10.1016/j.prostr.2020.12.004.

11. Islamgaliev R.K., Nikitina M.A., Ganeev A.V., Sitdikov V.D. Strengthening mechanisms in ultrafine-grained ferritic/martensitic steel produced by equal channel angular pressing // Material Science and Engineering: A. 2019. Vol. 744. P. 163–170. DOI: 10.1016/j.msea.2018.11.141.

12. Ivanisenko Y., Lojkowski W., Valiev R.Z., Fecht H.-J. The mechanism of formation of nanostructure and dissolution of cementite in pearlitic steel during high pressure torsion // Acta Materialia. 2003. Vol. 51. P. 5555–5570. DOI: 10.1016/S1359-6454(03)00419-1.

13. Ivanisenko Yu., MacLaren I., Sauvage X., Valiev R.Z., Fecht H.-J. Shear-induced α→γ transformation in nanoscale Fe-C composite // Acta Materialia. 2006. Vol. 54. P. 1659–1669. DOI: 10.1016/j.actamat.2005.11.034.

14. Shin D.H., Park K.-T., Kim Y.S. Formation of fine cementite precipitates in an ultra-fine grained low carbon steel // Scripta Materialia. 2003. Vol. 48. P. 469–473. DOI: 10.1016/S1359-6462(02)00512-2.

15. Vacchi G.D.S., Magalhães D.C.C., Kugelmeier C.L., Silva R. D., Mendes Filho A.D.A., Kliauga A.M., Rovere, C.A.D. Influence of long-term immersion tests on the electrochemical corrosion behavior of an ultrafine-grained aluminum alloy // Metals. 2024. Vol. 14(12). Art. 1417. DOI: 10.3390/met14121417.

16. Parfenov E.V., Kulyasova O.B., Mingo B., Farrahkov R.G., Cherneikina Y.V., Yerokhin A., Zheng, Y. F., Valiev R. Z. Influence of ultra-fine grain structure on corrosion behaviour of biodegradable Mg-1Ca alloy // Corrosion Science. 2020. Vol. 163. Art. 108303. DOI: 10.1016/j.corsci.2019.108303.

17. Nesterov K.M., Farrakhov R.G., Aubakirova V.R., Islamgaliev R.K., Sirazeeva A.R., Abuayyash A. Thermal stability and corrosion resistance of ultrafine-grained high-entropy Fe30Ni30Mn30Cr10 alloy // Frontier Materias & Technologies. 2022. Vol. 4. P. 81–89. DOI: 10.18323/2782-4039-2022-4-81-89.

18. Gubicza J., Ungár T. Characterization of defect structures in nanocrystalline materials by X-ray line

profile analysis // Zeitschrift für Kristallographie – Crystalline Materials. 2007. Vol. 222. P. 567–579. DOI: 10.1524/zkri.2007.222.11.567.

19. Ungár T., Dragomir I., Révész Á., Borbély A. The contrast factors of dislocations in cubic crystals: the dislocation model of strain anisotropy in practice // Journal of Applied Crystallography. 1999. Vol. 32(5). P. 992–1002. DOI: 10.1107/s0021889899009334.

20. Ledbetter H.M., Reed R.P. Elastic Properties of Metals and Alloys, I. Iron, Nickel, and Iron-Nickel Alloys // Journal of Physical and Chemical Reference Data. 1973. Vol 2. P. 531 DOI: 10.1063/1.3253127

21. Ungár T., Gubicza J., Ribárik G., Borbély, A. Crystallite size distribution and dislocation structure determined by diffraction profile analysis: principles and practical application to cubic and hexagonal crystals // Journal of Applied Crystallography. 2001. Vol. 34. P. 298–310. DOI: 10.1107/S0021889801003715.

22. Scardi P., Leoni, M. Whole Powder Pattern Modelling // Acta Crystallographica Section. 2002. A. Vol. 58. P. 190–200. DOI: 10.1107/S0108767301021298.

23. Wilkens M. The determination of density and distribution of dislocations in deformed single crystals from broadened X-ray diffraction profiles // Physica Status Solidi. 1970. Vol. 27. No. 2. P. 359–370. DOI: 10.1002/PSSA.19700020224

24. Ungár T., Gubicza J., Hanák P., Alexandrov I. Densities and character of dislocations and size-distribution of subgrains in deformed metals by X-ray diffraction profile analysis // Material Science and Engineering: A. 2001. Vol. 319–321. P. 274-278. DOI: 10.1016/S0921-5093(01)01025-5.

25. Ungár T., Ribárik G., Balogh L., Thomas R., Koc O., Preuss M., Race C.P., Frankel P. Fractional densities and character of dislocations in different slip modes from powder diffraction patterns // Journal of Nuclear Materials. 2024. Vol. 589. Art. 154828. DOI: 10.1016/j.jnucmat.2023.154828.

26. B. Baretzky, Baro M.D., Grabovetskaya, G Gubicza J., et. al. Fundamentals of interface phenomena in advanced bulk nanoscale materials // Reviews on Advanced Materials Science. 2005. Vol. 9. P. 45–108.

27. Ungár T. Dislocation densities, arrangements and character from X-ray diffraction experiments // Material Science and Engineering: A. 2001. Vol. 309–310. P. 14–22. DOI: 10.1016/S0921-5093(00)01685-3.

28. Miyamoto H. Corrosion of ultrafine grained materials by severe plastic deformation, an overview // Materials Transactions. 2016. Vol. 57. P. 559–572. DOI: 10.2320/matertrans.M2015452.